An Experimental-Cohesive Zone Model Approach to Predict Fatigue Life of Adhesive Joints with Varying Modes of Loading and Joint Configurations for Automotive Applications

Ahmed Hanafy Ibrahim[1], Brock Watson[1], Hamid Jahed[1], Saeid Rezaee[2], Duane S. Cronin[1*]

[1]*Department of MME, University of Waterloo, 200 University Avenue West, Waterloo, Canada*

[2]*Renault Group, Boulogne-Billancourt, France*

Abstract

Predictive fatigue life models of adhesive joints are necessary to enable the assessment of automotive bonded structures while reducing costly experimental testing. However, contemporary models have typically been calibrated for specific joint configurations and modes of loading, limiting their applicability to large-scale structures. Additionally, available models are based on simulation of cumulative fatigue cycling, making them computationally prohibitive. In the current study, fatigue experimental tests were undertaken on adhesive joints in cross-tension (CT) (load angles of 0°, 45°, and 90°) and single-lap shear joint (SLJ) configurations. A total of nine joint configurations, having symmetrical (same material and thickness) and asymmetrical (dissimilar material or unequal thickness) joints, were tested. Fatigue tests at load levels between 25-75% of the static peak load were performed until joint failure or to runout (two million load cycles). The static tests of the joints were simulated to failure using finite element (FE) models with the cohesive zone method (CZM). The maximum fracture energy release rates ($G_{\max}$) were calculated within the adhesive bond line at static loads corresponding to the peak loads of the fatigue tests. The $G_{\max}$ values, computed from single cycle, specimen-specific FE simulations, were correlated with the measured fatigue life

(N_f) of the adhesive joints with varying modes of loading and joint configurations. The fatigue life prediction model, based on $G_{max} - N_f$ correlation, predicted the cycles to failure for 85% of the fatigue tests, and 81% of the independent validation tests. The proposed fatigue life prediction approach provides computational efficiency and large-scale compatibility.

Keywords: adhesive fatigue life prediction, adhesive joints in automotive, adhesive cohesive zone model, fatigue testing of adhesive, adhesive finite element model

1. Introduction and Background

Structural adhesives are critical for multi-material joining and enabling the adoption of lightweight materials (*e.g.*, aluminum, ultra-high-strength steel, and composites) in future vehicles.[1] The use of adhesive joining in automotive structures has been reported to enhance load transfer, crashworthiness, and joint sealing while improving noise, vibration and harshness (NVH).[2, 3] Importantly, adhesively joined structures have demonstrated higher joint strength and fatigue life relative to spot welding and mechanical fastening.[4, 5] The existing predictive methods for estimating the fatigue life of adhesive joints have often been calibrated to specific tests and have generally required computationally expensive simulations of cumulative fatigue cycling,[6–8] lacking compatibility with large-scale structures (*e.g.,* automotive components).

Fatigue life prediction for adhesive joints can reduce the number of design iterations and amount of prototype testing of adhesively joined structures.[9] Early fatigue life prediction methods based on the stress-life approach were found to have limitations in accounting for joint geometry and mixed-mode loading.[10] In contrast, the fracture mechanics-based approach has been shown to account for mode mixity and joint geometry in the computation of the fracture energy release rate (G).[8, 11] Using the fracture mechanics approach, adhesive joints have been shown to exhibit a correlation between the fatigue crack growth (FCG) rate (da/dN) and G, also known as strain energy release rate (SERR).[2, 8, 12] The FCG-G correlation was reported

to demonstrate threshold, linear and fast fracture regions (Figure 1). In the linear region (Linear Region, Figure 1), the adhesive FCG rate has been related to G, using the Paris law,[11]

$$\frac{da}{dN} = C\, f(G)^m \tag{1}$$

Where a is the crack size, N is the number of cycles, C and m are experimental fitting coefficients and $f(G)$ is a function of the fracture energy release rate with various functions proposed in the literature, including:

$$f(G) = \Delta G = G_{max} - G_{min}, \text{[8]} \tag{2}$$

$$f(G) = G_{max}, \text{[11] and} \tag{3}$$

$$f(G) = \frac{G_{max}}{G_c} \text{[11]} \tag{4}$$

Where G_{max} and G_{min} are the fracture energy release rates corresponding to maximum and minimum cyclic loads, respectively, and G_c is the critical fracture energy release rate. A G_{max} below a certain threshold (G_{th}) would result in an extremely large fatigue life (approaching infinity), due to the absence of FCG (Threshold Region, Figure 1). G_{max} values close to the critical fracture energy release rate (G_c) would result in a rapid FCG rate and consequently a substantially low fatigue life (Fracture Region, Figure 1).

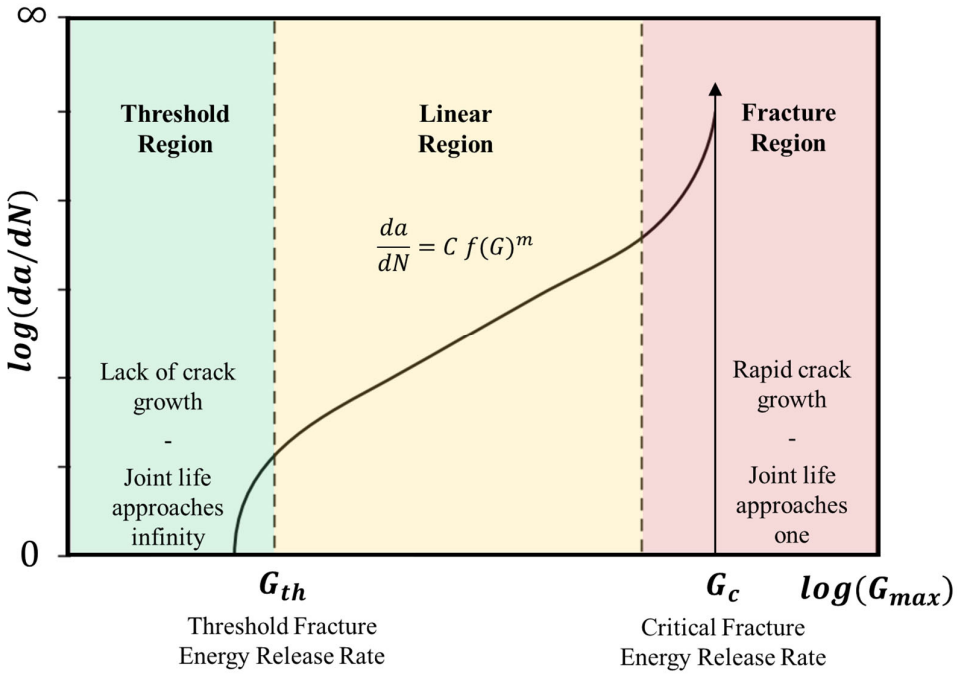


Figure 1: The FCG rate of a typical adhesive as a function of fracture energy release rate. Adapted from Abdel Wahab.[2]

Cohesive zone models (CZMs) can efficiently predict the fracture behavior of adhesive joints by allowing a crack to propagate within the cohesive elements when G reaches the critical value G_c.[13] The CZM approach has been used in finite element (FE) models to investigate the influence of joint configuration,[14] adherend and adhesive material,[15, 16] and loading conditions[10, 17, 18] on the mechanical response of adhesive joints. Several traction-separation responses are available to describe the CZM constitutive relationship using traction (T), separation (δ) and G, enabling 3D modelling of adhesive joints with and without an initial crack.[8] A bilinear (triangular) traction-separation response (Figure 2a) has been suggested for brittle and moderately ductile adhesives, and has been used in adhesive fatigue prediction studies because it was more computationally efficient and less susceptible to computational instabilities relative to more complex shapes (*e.g.*, trapezoidal).[17]

Predicting the fatigue life of adhesive joints by accounting for the adhesive FCG within the CZM formulation was proposed in the literature. Turon et al. proposed and validated a

fatigue life prediction approach for bonded specimens under Mode I, Mode II and mixed-mode loading, which was limited to specimen geometries with analytical expressions to calculate G.[6] The approach was enhanced to compute G from FE simulations using the internal strain energy and work from external forces, enabling its application to more complex geometries.[8] However, a user-defined cohesive element was required to incorporate the effect of the cyclic loading into the FE simulation by reducing the CZM parameters and traction-separation response with the load cycle count (Figure 2b).[7] In addition, the approach was only applied to specific test specimens, such as double cantilever beam (DCB) and SLJ, and was not assessed under mixed mode loading or high cycle fatigue.

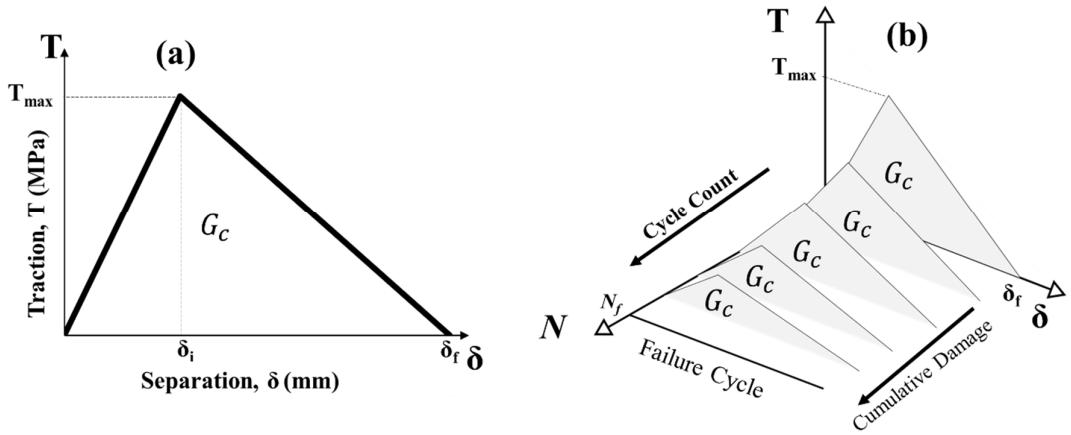


Figure 2: Bilinear traction-separation response (a), and the traction-separation response reduction with load cycle count (cumulative damage) (b). adapted from Costa et al.[7]

Previous fatigue life prediction approaches require simulating fatigue load cycling and adopting extensively modified CZM formulations, which in turn require prohibitively expensive computational resources for high cycle fatigue and are difficult to integrate within large-scale structural FE models (*e.g.,* vehicle models). Thus, a simplified adhesive reliability approach has been widely used in the automotive industry,[9] combining experimental, analytical and FE methods. The reliability approach used a reserve factor (*i.e.,* a safety factor based on infinite life) that was defined as a function of G_{max} and G_{th} computed from the static or cyclic FE simulation results. The use of static simulation results (single load cycle) to

identify a safe design, drastically improved the computational efficiency and compatibility with large-scale models; however, the approach was not extended to enable fatigue life estimation. Also, the computation of G required assuming or calibrating multiple parameters, which may limit its applicability to specific test specimens, modes of loading or adherend configuration.

In a previous study,[19] the static testing and FE modeling of adhesive joints with varying joint configurations and modes of loading were undertaken, providing a basis for the specimen geometries and adhesive used in the current study. A one-part epoxy-based structural adhesive (BetaGuard CI6125R; PPG, France) was characterized using the rigid double cantilever beam (RDCB) and bonded shear specimen (BSS) to measure the adhesive strength and toughness under Mode I and Mode II.[19–21] The experimental data were fitted to bilinear traction-separation responses to extract the CZM parameters (stiffness, peak traction and critical fracture energy release rate)(Figure 3). Following the material-level adhesive characterization, adhesively joined SLJ and CT specimens were tested to failure to measure the static force-displacement response, assessing the influence of mode mixity and joint configuration. Finally, the CZM parameters measured from the RDCB and BSS tests were used to model the adhesive joints to failure without the need to calibrate the CZM parameters. The simulation results were validated using the measured force-displacement data (Table 1) and optical measurements of SLJ joint rotation to validate the global response and local kinematics of the static FE models.

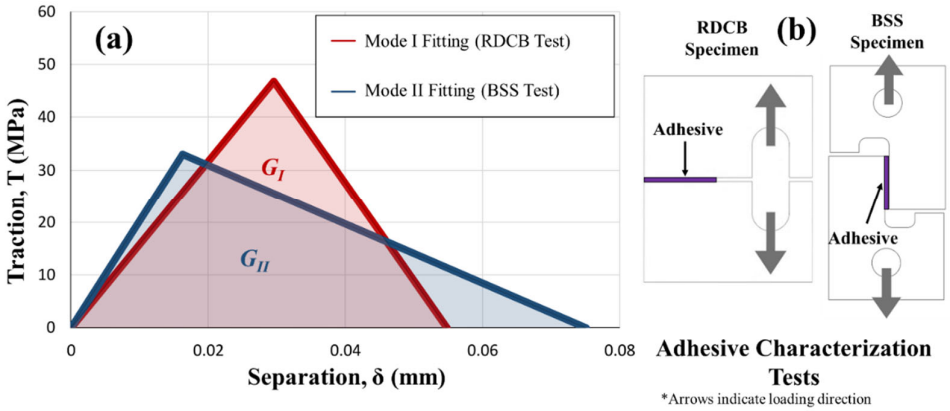


Figure 3. Cohesive traction-separation relationship for the BetaGuard CI6125R adhesive (a), and the RDCB and BSS specimens used for adhesive material-level characterization (b).[19]

Table 1. The measured and FE predicted static peak load of the SLJ and CT joint configurations[19]

Specimen Type	Adherend Configuration	Measured Static Peak Load (kN)	Predicted Static Peak Load (kN)
	Joint configurations used in the fatigue characterization tests		
SLJ	1 mm Al - 1 mm Al	6.16 ± 0.14	6.74
	1 mm Al - 2 mm Al	6.50 ± 0.07	7.08
	1 mm Al - 1.5 mm Steel	5.56 ± 0.31	7.30
0° CT	1 mm Al - 1 mm Al	0.63 ± 0.05	0.71
	1 mm Al - 2 mm Al	1.08 ± 0.06	1.25
	1 mm Al - 1.5 mm Steel	1.15 ± 0.01	1.34
45° CT	1 mm Al - 1 mm Al	3.81 ± 0.06	3.91
	Independent joint configurations for model validation		
SLJ	2 mm Al - 2 mm Al	7.4 ± 0.22	8.55
90° CT	1 mm Al - 1 mm Al	7.22 ± 0.27	6.49

The current study investigated a combined experimental-CZM approach to predict adhesive joint fatigue life for various adhesive joint configurations under varying modes of loading using a single load cycle simulation. First, the fatigue response of adhesive SLJ and CT joints, made with metallic adherends, was measured experimentally using a load ratio (R) of 0.1. Then, specimen-specific FE models of the joints were developed to compute the G value within the adhesive layer from a static simulation to failure. The adhesive CZM element data

were then extracted to compute the fracture energy release rates under Mode I (G_I) and Mode II (G_{II}) at loads corresponding to the maximum loads of the fatigue load levels. The process was repeated for all the SLJ and CT test cases and the maximum total energy release rate ($G_{\max}$) was calculated and correlated with experimentally measured number of cycles to failure life (N_f). The fatigue life prediction model, based on $G_{max} - N_f$ correlation, was validated using two independent test conditions to assess the model under different loading conditions relative to the tests used in the correlation, demonstrating the applicability of the model to varying joint configurations and loading modes.

2. Experimental and Computational Modeling Methodologies

2.1. SLJ and CT Test Specimen Preparation

The SLJ and CT test specimens were prepared at the same time as those presented in a previous study on static testing (Figure 4), and therefore only a brief summary of specimen preparation is presented here.[19] Both SLJ and CT adherends had the same dimensions (38 mm wide and 125 mm long) and a joint overlap of 37.5 mm (Figure 4a and 4b). SLJ and CT test specimens were made with two cold-rolled sheet materials with varying sheet thickness to create symmetrical (same adherend thickness and material) and asymmetrical (different adherend thickness or material) joints. A 6000 series (Mg-Si) aluminum alloy (1 mm and 2 mm sheet thicknesses) and a high-strength low-alloy (HSLA) steel (1.5 mm sheet thickness) (Table 2) were used due to their wide use in automotive structures. The water-jet cut adherends were first degreased using acetone, cleaned with a lint-free cloth and then treated using a special coating mixture (*i.e.,* cleaning solvent and metal preservative) to mimic the automotive production environment.[19]

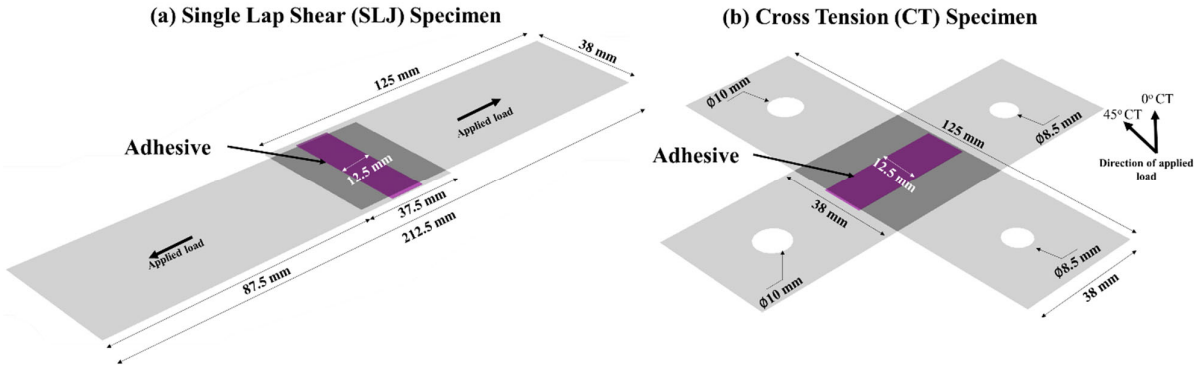


Figure 4. Adhesively bonded SLJ (a) and CT (b) test specimen geometries. (Adhesive layer in purple)

Table 2. Material properties of the adherends.

Adherend Properties	**Si-Mg Aluminum Alloy**	**HSLA Steel**
Density (kg/m^3)	2.71	7.8
Young's Modulus (GPa)	72	200
Poisson's Ratio	0.33	0.30
Yield Strength (MPa)	150	340

The adhesive (BetaGuard CI6125R; PPG, France) was applied in a continuous bead to the bond area of 12.5 mm x 38 mm, centered within the joint overlap length. Precise curing fixtures were used to ensure adherend alignment, apply a uniform clamping pressure, and to achieve a consistent bond line thickness, bond line length, and joint overlap. The curing fixtures were placed in a convection oven (ED-53, Binder, Tuttlingen, Germany) for 25 minutes at 180°C (excluding the ramp-up time) to cure the adhesive according to manufacturer specifications. Excess adhesive spew was removed with a file, and square tabs were bonded to the clamping regions of each test specimen to reduce load eccentricity. The bond line thickness (average of 0.297 ± 0.046 mm), bond line length (12.60 ± 0.10 mm), and joint overlap (37.95 ± 0.5 mm) were measured using an Opto-digital microscope (VHX-5000, Keyence, Japan) on the side of the SLJ specimens.

2.2. Fatigue Testing of SLJ and CT Specimens

The fatigue tests were conducted at room temperature on a servo-hydraulic tensile frame (8892; Instron, USA) with an integrated data acquisition system and a 25 kN load cell, with three repeats at each level. The SLJ specimens were mounted to the testing frame using hydraulic grips (Figure 5a) while the CT specimens required a custom testing apparatus that allowed for orienting the specimens at 0°, 45° and 90° relative to the applied load (Figure 5b). The maximum fatigue load level was 75% of the average static peak load,[19] which was reduced incrementally by 10-15% to multiple load levels achieving a fatigue life between 10,000 cycles and a runout of two million cycles.[22] Fatigue tests with life below 10,000 cycles required high loads that were outside the range of interest for automotive structures. The fatigue loading was applied as a sinusoidal waveform with a load ratio (R) of 0.1 and a loading frequency between 15 Hz for the SLJ, 45° CT and 90° CT. The loading frequency was reduced to 5 Hz for all the 0° CT tests to avoid sinusoidal wave distortion that occurred in this configuration due to relatively higher specimen compliance.

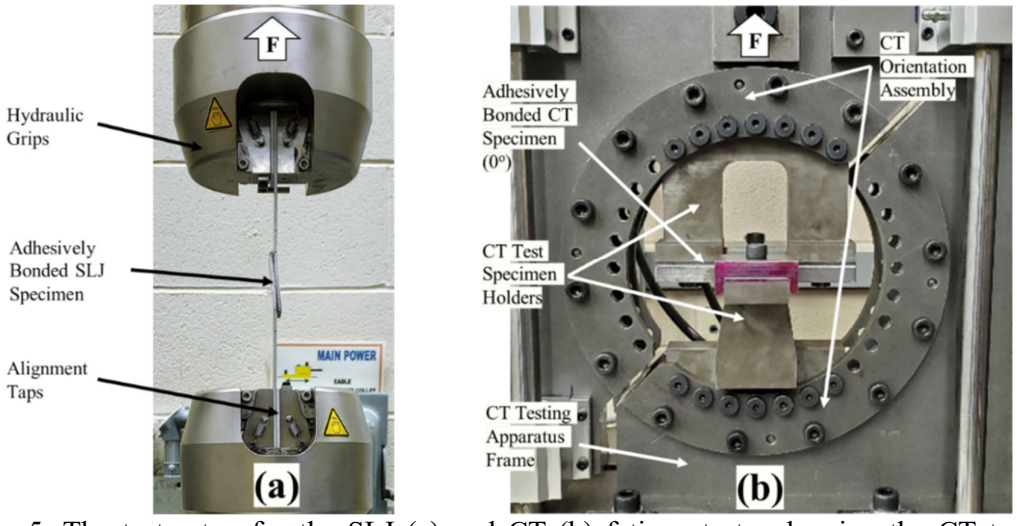


Figure 5. The test setup for the SLJ (a) and CT (b) fatigue tests, showing the CT testing apparatus. F indicates the direction of the applied load.

The fatigue testing matrices comprised two sets of tests with varying joint configurations and modes of loading. Seven configurations (three SLJ, three 0° CT, and one

45° CT configuration) were tested to develop the fatigue life prediction model by correlating the measured fatigue life and fracture energy release rate computed from FE models (Table 3). Additionally, two independent joint configurations, using an adherend configuration and a loading condition that were not used in the fatigue life prediction model development, were tested for validation of the model (Table 4). The joint configurations varied adherend material, adherend thickness (1 mm being common to all joint configurations) and loading angle.

Table 3. The SLJ and CT fatigue characterization test matrix, used for the fatigue life prediction model development, included varying modes of loading and joint configurations.

Specimen	**Load Level**	**Adherend Configuration** *1 mm Al* *1 mm Al*	*1 mm Al* *2 mm Al*	*1 mm Al* *1.5 mm Steel*
SLJ	75%	X	X	X
	65%	X	X	X
	55%	X	X	X
	40%	X	X	
0° CT	75%	Life below 10,000 cycles	Life below 10,000 cycles	Life below 10,000 cycles
	65%	Life below 10,000 cycles	Life below 10,000 cycles	Life below 10,000 cycles
	55%	X	X	X
	40%	X	X	X
	25%	X	X	X
45° CT	75%	Life below 10,000 cycles		
	65%	X		
	55%	X		
	40%	X		

Table 4. The SLJ and CT fatigue test matrix used for validation of fatigue life prediction model.

Specimen	**Adherend Configuration**	**Load Levels**
SLJ	2 mm Al - 2 mm Al	70%, 60%, 50%, 45%
90° CT	1 mm Al - 1 mm Al	75%, 65%, 55%, 40%

2.3.Development of Fatigue Life Prediction Model for Adhesive Joints

The development of the fatigue life prediction model consisted of four successive steps (Figure 6):

(1) Conducting fatigue testing on adhesive joints using SLJ and CT tests with varying joint configurations (*i.e.,* adherend thickness and material) and loading angles (*i.e.,* loading modes), supplemented with previous quasi-static testing.

(2) Development and validation of specimen-specific FE models of the static tests using CZM, based on material-level characterization tests (*e.g.,* RDCB and BSS tests - see Ibrahim et al.[19]).

(3) Computation of the fracture energy release rates (G_I, G_{II}) for each cohesive element in the FE static simulation results at loads corresponding to the peak loads of fatigue tests, and then determining G_{max} among all elements at a given load level.

(4) Correlation of the computed G_{max} and N_f measured from the experimental characterization tests, followed by fatigue life prediction model validation using an independent set of tests.

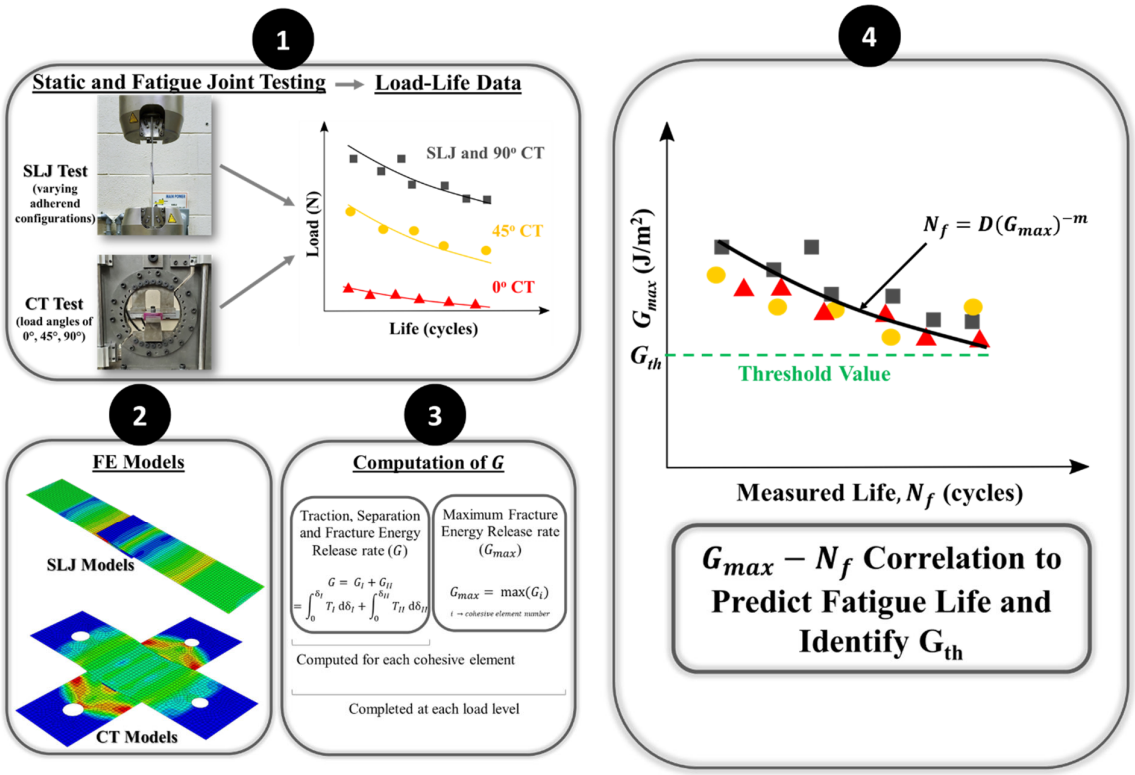


Figure 6. Illustration of the development of the fatigue life prediction model to estimate the fatigue life of adhesive joints with varying modes of loading and joint configurations.

2.4. Development and Validation of Specimen-specific FE Models

The development of the FE models of the SLJ (Figure 7a) and CT (Figure 7b) tests followed the same methodology laid out in a previous study.[19] A commercial finite element program (ABAQUS Standard 2018; Simulia, Dassault Systemes) was used to develop the specimen models using fully integrated shell elements for adherends (2 mm x 2 mm) and CZM elements for the adhesive (1 mm x 1 mm).[19] A script was developed using Python™ (version 2.7.0), ABAQUS Scripting Interface and array programming with Numpy[23] (version 1.6.2) to extract the traction-separation data for each cohesive element in the bond area from the static simulation results at load levels corresponding to the peak loads of the fatigue tests (Table 3). The FE models were used to quantify the local (*i.e.,* cohesive element level) mode mixity and to assess the effect of cohesive element size and adherend material model on the locally computed G and consequently fatigue life prediction model accuracy.

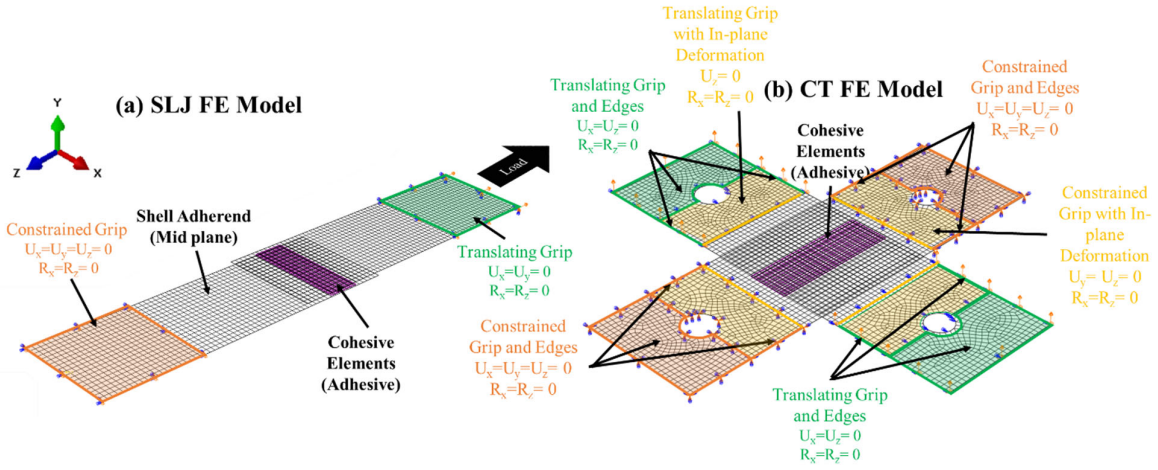


Figure 7. FE models for SLJ (a) and CT tests (b), illustrating the mesh, boundary conditions, adhesive CZM, and adherend shell elements.

2.5. Computation of the Fracture Energy Release Rates and $G_{max} - N_f$ Correlation

The fracture energy release rate (G) was computed for each cohesive element in the bond line for each specimen-specific FE model, based on the area under normal (Mode I) and tangential (Mode II) traction-separation responses reported for each element using,

$$G_I = \int_0^{\delta_I} T_I \, d\delta_I \quad (5)$$

$$G_{II} = \int_0^{\delta_{II}} T_{II} \, d\delta_{II} \quad (6)$$

where T_I, T_{II}, δ_I and δ_{II} are the traction and separation values within a cohesive element under Mode I and Mode II, respectively. Each cohesive element contained four node pairs (*i.e.,* integration points), so the traction and separation values for each cohesive element were averaged for each mode of loading (*i.e.,* averages of four traction and four separation values for each mode of loading). To account for mixed modes of loading, G has been defined in the literature as G_I, G_{II} or $G_I + G_{II}$.[24] In the current study, $G_I + G_{II}$ was used because it offered conservative estimates of the combined G value and acknowledged that the crack driving force was due to both Mode I and Mode II loading, which was observed in the static simulations.[19]

The total fracture energy release rate for each cohesive element was then calculated from the average traction and separation values as follows, [17]

$$G = G_I + G_{II} = \int_0^{\delta_I} T_I \, d\delta_I + \int_0^{\delta_{II}} T_{II} \, d\delta_{II} \quad (7)$$

After calculating G for each cohesive element, G_{max} was determined by identifying the greatest G value among all the elements using,

$$G_{max} = \max(G) \qquad \{\text{over all elements within bond line}\} \quad (8)$$

Because adhesive crack initiation (nucleation) typically represents a small amount of the fatigue life and ends during early loading cycles,[24] the FCG rate primarily occurs during the crack propagation phase (Paris law, Eq.1). Using Eq. 3,[11] the Paris law (Eq. 1) could be rewritten to define the FCG rate as,

$$\frac{da}{dN} = C(G_{max})^m \quad (9)$$

where G_{max} was computed from the FE simulation (Eq. 8 above). The FCG rate was assumed to be a function of the maximum fracture energy release rate exhibited locally within the

adhesive bond line, and the number of cycles to failure (N_f) for a known bond line area (Δa) could be estimated using,[7, 17]

$$N_f = \frac{\Delta a}{\frac{da}{dN}} \tag{10}$$

The correlation between experimentally measured N_f and G_{max} values, computed from the specimen-specific FE models at each load level, could be expressed as,

$$N_f = \begin{cases} 1 & G_{max} \geq G_c \\ \mathrm{D}\,(G_{max})^{-m} & G_{th} < G_{max} < G_c \\ \infty & G_{max} < G_{th} \end{cases} \tag{11}$$

where $\mathrm{D} = \frac{\text{bond line area}}{C}$, and C and m were fitting coefficients in Eq. 9.

3. Results and Discussion

3.1. SLJ and CT Fatigue Characterization Tests

The fatigue behavior of the adhesively bonded joints (SLJ and CT) made with varying adherend materials (aluminum and steel) and adherend thickness (

Figure 8) exhibited dependency on the specimen geometry and mode of loading, owing to the sensitivity of adhesive joint strength to loading orientation and adherend deformation. The adhesive fatigue life was highest in the SLJ specimens, and lowest in the 0° CT tests, among all load levels.

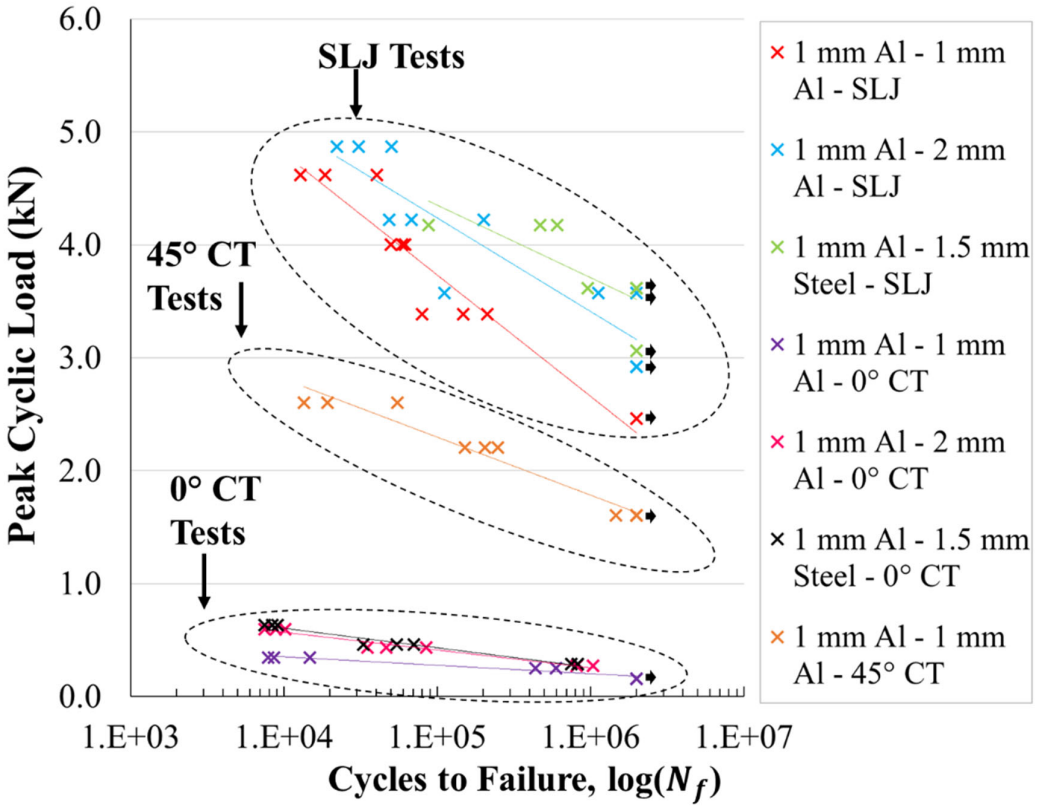


Figure 8. Load-Cycles to failure (N_f) data for the fatigue characterization tests (SLJ, 45° CT and 0° CT). Arrows indicate fatigue life greater than two million cycles (runout).

The SLJ tests with symmetric and asymmetric adherend configurations covered a range of fatigue lives from 10,000 cycles to runout (*i.e.,* 2 million cycles). The joints exhibited rotation within the overlap area and localized in-plane deformation (i.e., stretching along length and width reduction) within the 1 mm Al adherend at the joint free ends before failure. The fatigue crack was observed to initiate within the adhesive layer, at one of the adhesive free ends (Figure 9a). The initial crack growth rate was modest and challenging to monitor optically. Once past initiation, the crack propagated at a modest rate throughout the bond line length, and then the FCG rate increased rapidly within the last few thousand cycles before failure, resulting in an abrupt joint failure. The failure surfaces generally demonstrated shear failure with a sharp transition zone near the center line of the bond line length, which was also reported for similar joints under static loading.[19, 25]

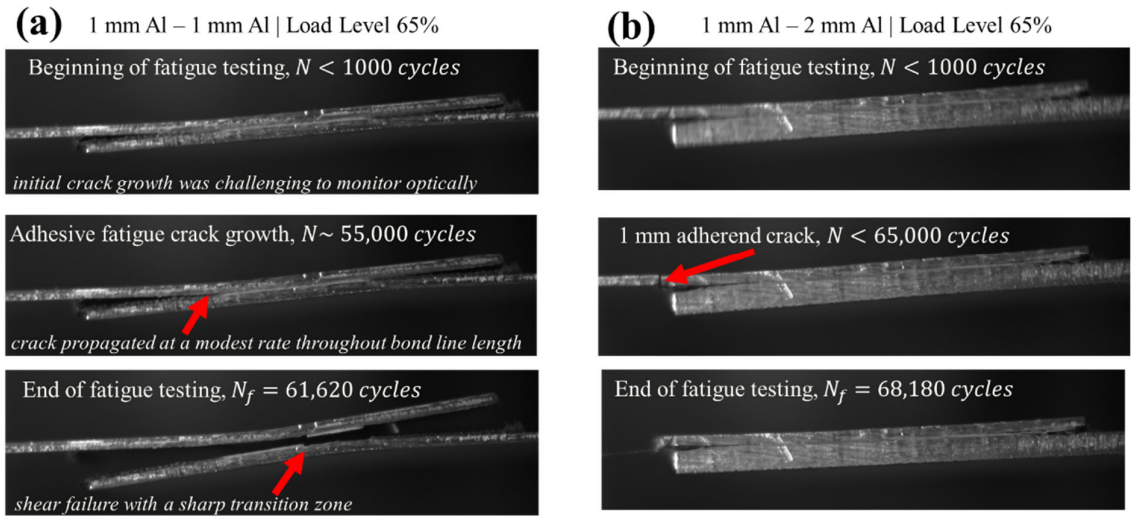


Figure 9. SLJ side view showing crack initiation and propagation during cohesive failure (a) and adherend failure (b).

Asymmetrical SLJ joints generally exhibited higher fatigue life relative to the symmetrical joints. The fatigue life demonstrated dependency on adherend thickness and material, with thicker adherends presenting a somewhat higher number of cycles to failure. The 1 mm Al - 2 mm Al joints exhibited higher fatigue life, within a factor of two, relative to the 1 mm Al - 1 mm Al joints, and the 1 mm Al - 1.5 mm steel demonstrated the highest number of cycles to failure. The influence of adherend thickness and material was also manifest in the fatigue load level corresponding to runout. The runout life occurred at a fatigue load level of 40% of the static peak load for 1 mm Al - 1 mm and 55% load level for the Al and 1 mm Al - 2 mm Al and 1 mm Al - 1.5 mm steel joints, highlighting that the asymmetrical joints could achieve runout at higher load levels. Although increased adherend thickness showed an increase in the number of cycles to failure, asymmetrical joints showed higher variability owing to adherend failure in the 1 mm Al adherend. The asymmetrical joint demonstrated susceptibility to adherend failure in the thin adherend at load levels above 50% (Figure 9b). The change in failure mechanism, from shear failure within the adhesive layer to adherend failure, could be attributed to the 1 mm Al adherend exhibiting highly localized strains due to

combined bending and in-plane deformation (stretching and width reduction), close to the adhesive free ends.[19]

The 0° CT specimen exhibited the lowest cycles to failure relative to SLJ and 45° CT joints with the same joint configuration and load level. The joints were highly sensitive to the load level such that a small change to the load level resulted in a drastic difference in fatigue life. For all 0° CT tests (symmetrical and asymmetrical joints), the crack initiated at the adhesive boundaries due to peeling as the 1 mm adherend exhibited substantial bending deformation at the boundaries of the joint overlap. At the 75% and 65% load levels, the adherend bending resulted in a fatigue life below 10,000 cycles in both symmetrical and asymmetrical joints. Decreasing the load level to 55% caused a modest increase in the fatigue life of the symmetrical and asymmetrical joints, which failed at about 10,000 cycles. Further reduction in the load level to 40% led to substantially higher fatigue life for the symmetrical joints than the asymmetrical joints (up to 10 times higher, ~500,000 cycles versus 50,000 cycles). The bending deformation in the 1 mm adherend was more pronounced in the asymmetrical joints, resulting in an early crack growth and premature adhesive joint failure. Thus, the asymmetrical joints could not achieve runout (two million cycles), even at a load level of 25% and failed at roughly one million cycles. In contrast, the symmetrical joints consistently achieved run out for the same load level, highlighting that the fatigue life of adhesive joints was dependent on joint configuration and adherend deformation.

The 45° CT tests exhibited fatigue lives that were lower than those of SLJ tests but higher than the 0° CT tests at similar load levels. For example, at a 40% load level, the 45° CT tests had four times the fatigue life of 0° CT, and the factor increased at higher load levels. The load-cycles to failure data showed low scatter and less variability relative to the 0° CT tests across the fatigue life range, which could be attributed to the reduced adherend bending deformation under this loading orientation. While the 0° CT exhibited localized deformations,

the 45° CT showed modest bending deformation within the adherends, thus, the mixed mode loading was uniformly distributed among the bond area. The CT specimen testing device reduced undesirable joint rotation and out-of-plane displacement, which helped achieve consistent mixed mode loading and adherend deformation, and consequently fatigue results with low variability.

3.2. SLJ and CT Fatigue Life Prediction Model Validation Tests

The experimental tests used to validate the fatigue prediction model (*i.e.,* $G_{max} - N_f$ correlation) included SLJ and 90° CT tests (Figure 10). The test peak cyclic loads ranged from 2.9 to 5.8 kN, and covered fatigue lives between 10,000 cycles up to runout (2 million cycles). The SLJ tests used a sheet thickness (2 mm to 2 mm) that was not used in prediction model development, which reduced adherend deformation and enabled validating the fatigue life prediction model against higher fatigue peak loads relative to the tests with 1 mm aluminum adherends. The 90° CT joints loaded the adhesive along the bond line width, as opposed to loading the adhesive along the bond line length, which created a distinct failure surface and crack growth path within the bonding area compared to SLJ.[19] Importantly, the validation tests assessed the prediction model under different loading conditions relative to the tests used for model development.

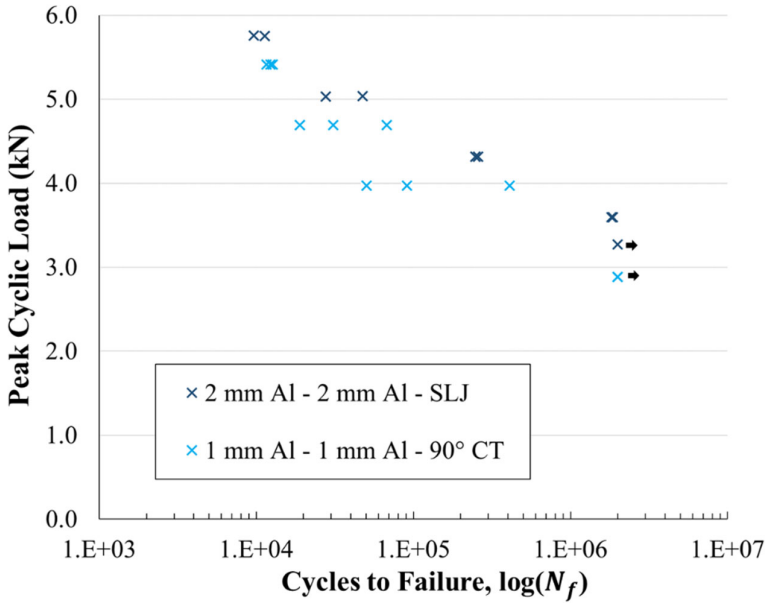


Figure 10. Load-Cycles to failure (N_f) data for the fatigue life prediction model validation tests (SLJ and 90° CT tests).

3.3. Fracture Energy Release Rate Computation and $G_{max} - N_f$ Correlation

After processing the static FE models, the calculated G_{max} values were plotted versus the experimentally measured cycles to failure, N_f, for the SLJ, 45° CT and 0° CT joints, using a log-log scale and excluding runout tests. Linear regression models demonstrated strong correlations ($R^2 > 0.8$) to the log-log data. The threshold values at which the life of the joint reached runout could be estimated from the G_{max} - N_f curves (Figure 11a). The average threshold value (G_{th}) for SLJ (Mode II), 0° CT (Mode I) and 45° CT (mixed mode) joints was 74 J/m^2 (range between 60 J/m^2 to 85 J/m^2), and the threshold value demonstrated some level of dependency on loading mode. The 0° CT exhibited the lowest threshold value of 60 J/m^2 while SLJ specimens showed a somewhat higher threshold value of 75 J/m^2. A previous study reported similar threshold values (below 70-85 J/m^2) for a structural epoxy adhesive using SLJ and coach peel specimens.[9] Threshold values were often reported in the literature using fracture tests (DCB and end-notched flexure test (ENF)) and ranged between 10% of G_c to 55% of G_c with values closer to 10% of G_c more common.[7, 12, 26, 27] In the current study, the joints

demonstrated a G_{th} closer to 6 - 7% of G_c, attributed to the higher bending deformation and localized loading in joint tests compared to traditional fracture test specimens.

The FCG rate predicted using Eq. 9 and the computed G_{max} values followed a typical Paris law regardless of adherend configuration (Figure 11b), highlighting that the G_{max} computations from static FE models were physical and followed the same behavior generally measured from experimental fracture tests under cyclic loading (*e.g.,* DCB test). Computing the fracture energy release rate from cohesive elements offered key advantages over previous studies that used analytical methods (*e.g.,* beam theory or J-Integral), such as accounting for adherend deformations (*e.g.,* bending observed in CT tests and SLJ joint rotation) with a high level of accuracy.

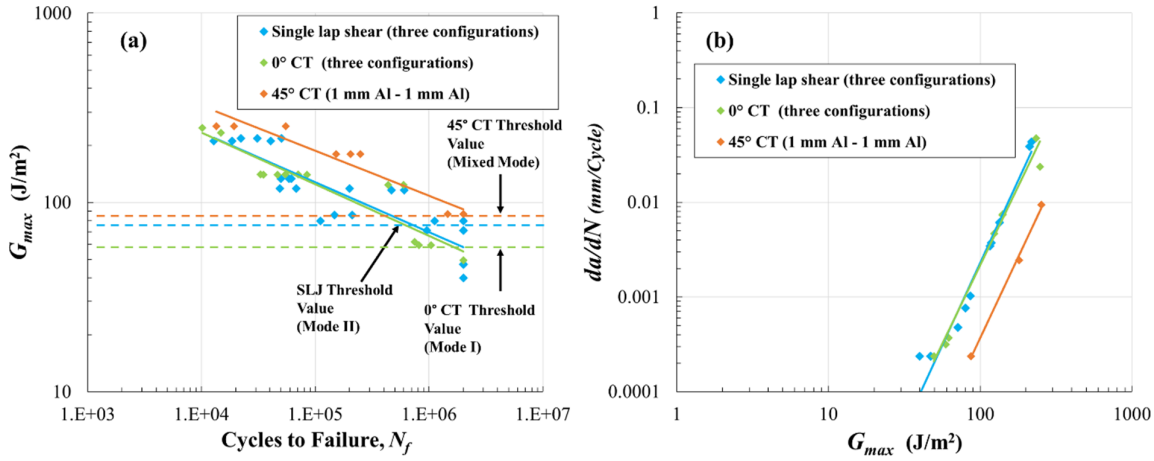


Figure 11. The $G_{max} - N_f$ data for the fatigue characterization tests (SLJ, 45° CT and 0° CT) (a) and the predicted FCG rate using Eq. 9.

The local mode mixity within the specific G_{max} element for each specimen-specific simulation was quantified for the (SLJ, 45° CT and 0° CT) with symmetrical joint configuration (1 mm Al – 1 mm Al adherends). The mode ratio ($\varphi = \tan^{-1}\sqrt{G_{II}/G_I}$) was calculated to shed light on the local crack growth driving mechanism (Table 5). The elements exhibiting G_{max} in SLJ models generally exhibited little to no mode mixity (local mode ratio > 81°, where 90° is pure Mode II) at all fatigue load levels (up to 75% of static load). The adherend in-plane

deformation (stretch and width reduction) of the 1 mm Al adherend reduced the localized bending at the adhesive free ends and consequently joint rotation, which reduced Mode I loading at the adhesive boundaries. Consequently, the cohesive element exhibiting G_{max} corresponded to the element exhibiting maximum traction under Mode II. In contrast, the 0° CT and 45° CT exhibited fatigue crack growth due to mixed mode loading. The 0° CT models experienced a mode ratio of up to 50° locally within the element exhibiting G_{max}, attributed to the substantial adherend bending at all load levels. The 45° CT mixed mode ratio agreed with the applied load angle (45°), and increased by a modest 2° at the highest load level due to the increased adherend deformation and joint rotation at higher loads.

Table 5. The mode mixity summary for the fatigue characterization models (SLJ, 45° CT and 0° CT) with symmetrical configuration, computed locally at the element experiencing G_{max}.

FE Model	Joint Configuration	Mode Ratio (degrees)	Crack Growth Mechanism	Element Experiencing G_{max}
SLJ	1 mm Al – 1 mm Al	> 81°	Pure Mode II	Corresponded to element experiencing maximum T_{II}
0° CT		< 50°	Mixed Mode	Corresponded to element experiencing maximum $G_I + G_{II}$
45° CT		45.3° - 47°	Mixed Mode	Corresponded to element experiencing maximum $G_I + G_{II}$

3.4. Master Curve and Validation of the $G_{max} - N_f$ Correlation using Independent Experimental Data

A master curve was constructed using the data points for all joint configurations used in fatigue characterization tests (three adherend configurations for SLJ and 0° CT specimens and one adherend configuration for the 45° CT specimen) (Table 3), excluding seventeen runout data points (Figure 12a). The $G_{max} - N_f$ data points were linearly correlated (after log-log transformation) regardless of the test specimen, joint configuration and mode of loading. The master $G_{max} - N_f$ regression model (Table 6) was used to predict the fatigue life and FCG rate for all the characterization tests to verify the model predictions. The predicted *da/dN* -

G_{max} relationship followed a typical Paris law (Figure 12b). The predicted *da/dN* - G_{max} relationship showed a relatively strong correlation (R^2 = 0.75), indicating that the approach followed in this research was able to account for the difference in joint geometry, joint configuration and mode of loading to a reasonable extent using the G_{max} values computed within the adhesive bond line.

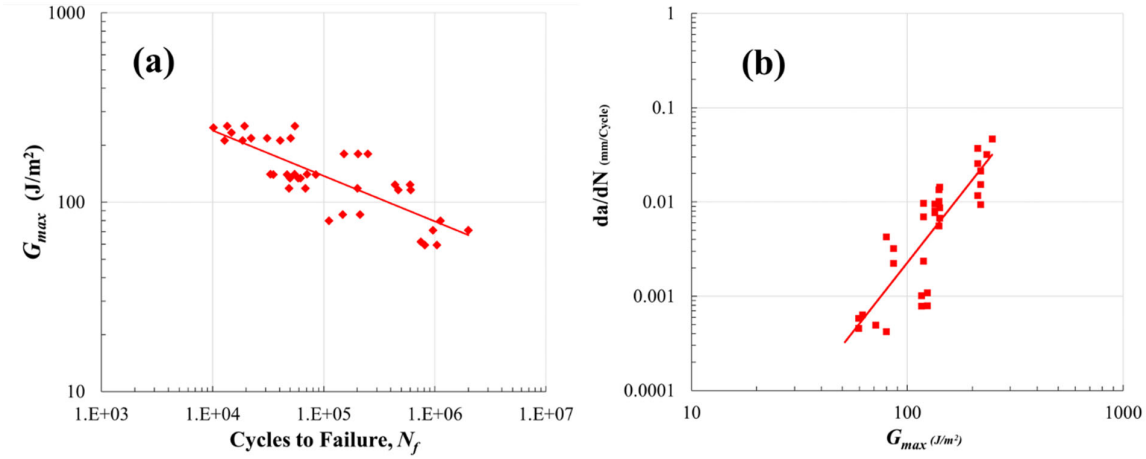


Figure 12. The master $G_{max} - N_f$ curve (a) and the predicted FCG rate versus computed G_{max} data (b) for the fatigue characterization tests (SLJ, 45° CT and 0° CT). (G_{max} computed from the specimen specific FE models at each load level)

Table 6. The master regression model using $G_{max} - N_f$ correlation for fatigue characterization tests with varying joint configurations and modes of loading (characterization tests).

Specimen geometry	Number of tests, excluding runout tests	Coefficient (D)	Exponent (m)	Average Threshold value (G_{th}, J/m²)
SLJ, 45° CT and 0° CT	41	2182	0.24	74

The model estimated the fatigue life of 85% of the fatigue characterization tests (SLJ, 45° CT and 0° CT, tests used in model development) within a factor of three (red square markers, Figure 13). Most of the tests that were not between the 3x scatter band were overpredicted, and was due to the 1 mm early adherend failure in SLJ tests (discussed in section

3.1). Importantly, the prediction model estimated the fatigue life for 81% of the validation tests (independent set of tests not used in model development) within the same 3x scatter band (blue square markers, Figure 13).

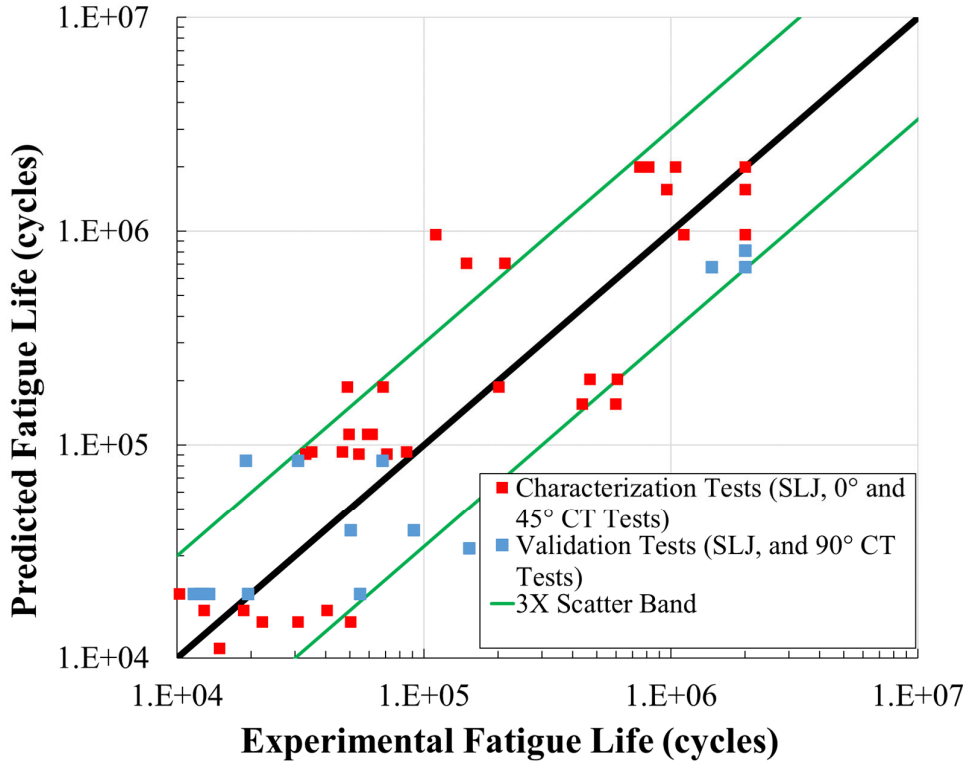


Figure 13. Validation of the master fatigue prediction model, based on $G_{max} - N_f$ correlation, showing the predicted and experimentally measured fatigue lives of model calibration tests (red) and validation tests (blue).

The fatigue life prediction model accuracy was assessed using the root mean square deviation (RMSD). The RMSD was calculated for the datasets from the fatigue characterization tests and validation tests using the methods laid out in the literature.[10] The calculated RMSD was 0.391 for the fatigue characterization tests, and 0.393 for the validation tests, indicating that the model performed similarly on adhesive joints that were not used in model development. Importantly, G_{max} values for all fatigue load levels of a joint configuration (*e.g.,* SLJ with 1 mm Al – 1 mm Al) were computed from a single cycle simulation, requiring an average CPU time of approximately 50 minutes per model, using a 4-core workstation with 8 threads. In

contrast, traditional methods using cyclic simulations often require 2000 times or more this CPU time (~100,000 minutes) to simulate a runout fatigue test using the same workstation, even when using a cycle jumping strategy[28] to reduce the number of simulated cycles. The targeted fatigue prediction bounds were appropriate for automotive applications (bounds of fatigue life prediction within a factor of three[10]), considering that the model provided sufficient flexibility to account for varying modes of loading and joint configurations across a large domain of fatigue lives (10,000 cycles to a runout of two million cycles). It is important to note that the model has some limitations including the use of a single adhesive and one fatigue load ratio (R).

3.5. Influence of Cohesive Element Size and Adherend Material Model on Fatigue Life Prediction

The size of the cohesive element plays a role in the convergence and accuracy of the response of adhesive joint FE models.[19, 29, 30] Therefore, the FE models of the validation tests (SLJ, made with 2 mm Al - 2 mm Al, and 45° CT) were simulated with cohesive elements having half (0.5 mm) and double (2 mm) the element size used for the original FE models with 1 mm cohesive elements, determined in a previous mesh sensitivity study.[19] Decreasing the element size to 0.5 mm caused a modest increase in the G_{max} value, between 12-17% depending on load level and loading mode and consequently had little influence on the fatigue life predictions (red markers, Figure 14a). In contrast, increasing the cohesive element size from 1 mm to 2 mm reduced the computed G_{max} value for all load levels regardless of the specimen geometry or loading mode (up to 43% reduction). Consequently, the prediction accuracy was considerably lower for both the SLJ and 45° CT tests, such that most of the tests were not predicted within a factor of three (yellow markers, Figure 14a). The prediction model accuracy was sensitive to large mesh size, emphasizing the importance of finding a middle ground between model accuracy and computational efficiency by using two to three cohesive

elements in the cohesive zone length (calculated as 1.7 mm) as recommended in the literature.[30]

The large-scale FE models developed for automotive fatigue analysis usually favor elastic material models, when appropriate, to improve computational efficiency. Using a perfectly elastic model to compute the G_{max} value influenced the predictions of 45° CT tests with higher load levels, which exhibited some adherend deformation (square markers, Figure 14b). However, SLJ and 45° CT tests with fatigue cycles above 100,000 cycles (lower load levels) showed limited influence for material model plasticity on joint fatigue life prediction (Figure 14b). Using an elastic-plastic material model played a key role in the development of the fatigue prediction model but the model implementation showed some flexibility toward the material model for lower load levels for tests with elastic adherend deformation.

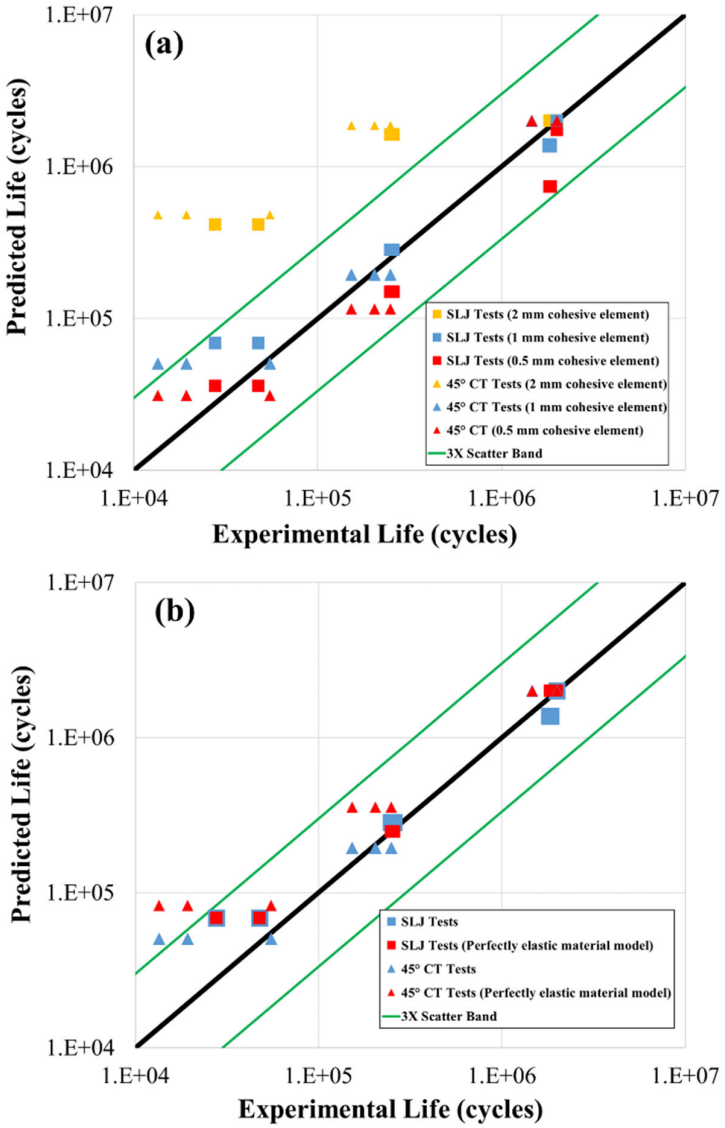


Figure 14. The influence of CZM element size (a) and adherend material model (b) on the fatigue life prediction.

4. Conclusion

The proposed fatigue life prediction approach was based on experimental material-level adhesive characterization, experimental adhesive joint fatigue testing, and specimen-specific static FE models with CZM to predict the fatigue life of adhesive joints. The fatigue load-life response of the SLJ, 0° CT and 45° CT exhibited dependency on the specimen geometry and mode of loading, owing to the sensitivity of adhesive joint strength to loading orientation and

adherend deformation. The adhesive fatigue life was highest in the SLJ specimens, and lowest in the 0° CT tests, among all load levels. In addition, joint configuration influenced the fatigue life of SLJ and CT specimens, highlighting that adhesive joint fatigue life was dependent on adherend thickness and material type.

Using static FE models with CZM enabled the computation of G_{max} at different load levels, without needing to simulate the computationally expensive fatigue cycling. Using the $G_{\max}$ values, computed locally within the adhesive bond line, and measured fatigue life, N_f, the $G_{max} - N_f$ response exhibited a linear correlation, after log-log transformation, regardless of mode of loading or joint configuration. The fatigue life prediction model, based on $G_{max} - N_f$ correlation, predicted the cycles to failure for 85% of the fatigue characterization tests (SLJ, 0° CT and 45° CT), and 81% of the independent validation tests, which assessed different adherend configurations and loading modes. The fracture energy release rate threshold value (an average of 74 J/m^2) was estimated from the $G_{max} - N_f$ correlation, which allowed the loads at which the adhesive joint fatigue life approached runout (> two million cycles) to be identified.

This work demonstrated an approach to predict the fatigue life of adhesive joints with different specimen geometry, joint configuration (adherend material and thickness) and loading conditions, without requiring simulating fatigue load cycling. The approach presented is compatible with large-scale models. In future work, a structural level validation using an automotive component will be conducted, and the approach will be extended to different types of adhesives while varying the fatigue load ratio.

5. Acknowledgement

The authors would like to thank the Renault Group for their support of this research [grant number REGIENOV DEA-TD-68193-18-169]. This research was undertaken, in part, thanks to funding from the Canada Research Chairs Program.

6. Declarations of Conflict of Interest

The authors report there are no competing interests to declare.

7. References

[1] Meschut, G.; Hahn, O.; Janzen, V.; Olfermann, T. Innovative Joining Technologies for Multi-Material Structures. *Weld. World*, **2014**, *58* (1), 65–75. https://doi.org/10.1007/s40194-013-0098-3.

[2] Abdel Wahab, M. M. Fatigue in Adhesively Bonded Joints: A Review. *ISRN Mater. Sci.*, **2012**, *2012* (c), 1–25. https://doi.org/10.5402/2012/746308.

[3] Lanzerath, H.; Pasligh, N. Benefit of Structural Adhesives in Full Car Crash Applications. *SAE Tech. Pap.*, **2014**, *2014-01–08*. https://doi.org/10.4271/2014-01-0811.

[4] Wang, P. C.; Chisholm, S. K.; Banas, G.; Lawrence, F. V. Role of Failure Mode, Resistance Spot Weld and Adhesive on the Fatigue Behavior of Weld-Bonded Aluminum. *Weld. J. (Miami, Fla)*, **1995**, *74* (2), 41-s.

[5] Ibrahim, A. H.; Cronin, D. S. Mechanical Testing of Adhesive, Self-Piercing Rivet, and Hybrid Jointed Aluminum under Tension Loading. *Int. J. Adhes. Adhes.*, **2022**, *113* (June 2021), 103066. https://doi.org/10.1016/j.ijadhadh.2021.103066.

[6] Turon, A.; Costa, J.; Camanho, P. P.; Dávila, C. G. Simulation of Delamination in Composites under High-Cycle Fatigue. *Compos. Part A Appl. Sci. Manuf.*, **2007**, *38* (11), 2270–2282. https://doi.org/10.1016/j.compositesa.2006.11.009.

[7] Costa, M.; Viana, G.; Créac'hcadec, R.; da Silva, L. F. M.; Campilho, R. D. S. G. A Cohesive Zone Element for Mode I Modelling of Adhesives Degraded by Humidity and Fatigue. *Int. J. Fatigue*, **2018**, *112*, 173–182. https://doi.org/10.1016/j.ijfatigue.2018.03.014.

[8] Pirondi, A.; Moroni, F. A Progressive Damage Model for the Prediction of Fatigue Crack Growth in Bonded Joints. *J. Adhes.*, **2010**, *86* (5–6), 501–521. https://doi.org/10.1080/00218464.2010.484305.

[9] Heyes, P.; Björkman, G.; Blows, A.; Mumford, T.; Briskham, P. A Fracture Mechanics Approach to Durability Calculations for Adhesive Joints. *SAE Int. J. Mater. Manuf.*, **2012**, *5* (1), 215–225. https://doi.org/10.4271/2012-01-0731.

[10] Antelo, J.; Akhavan-Safar, A.; Carbas, R. J. C.; Marques, E. A. S.; Goyal, R.; da Silva,

L. F. M. Fatigue Life Evaluation of Adhesive Joints in a Real Structural Component. *Int. J. Fatigue*, **2021**, *153* (July), 106504. https://doi.org/10.1016/j.ijfatigue.2021.106504.

[11] Santos, D.; Carbas, R. J. C.; Marques, E. A. S.; Wenig, S.; Silva, L. F. M.; Carbas, R. J. C.; Marques, E. A. S.; Wenig, S. Mode I Fatigue Threshold Energy Assessment of a Polyurethane Adhesive : Effects of Temperature and Paris Law Relation. *J. Adhes.*, **2023**, *00* (00), 1–25. https://doi.org/10.1080/00218464.2023.2225415.

[12] Kinloch, A. J.; Osiyemi, S. O. Predicting the Fatigue Life of Adhesively-Bonded Joints. *J. Adhes.*, **1993**, *43* (1–2), 79–90. https://doi.org/10.1080/00218469308026589.

[13] Park, K.; Paulino, G. H. Cohesive Zone Models: A Critical Review of Traction-Separation Relationships across Fracture Surfaces. *Appl. Mech. Rev.*, **2011**, *64* (6). https://doi.org/10.1115/1.4023110.

[14] Khoramishad, H.; Crocombe, A. D.; Katnam, K. B.; Ashcroft, I. A. Predicting Fatigue Damage in Adhesively Bonded Joints Using a Cohesive Zone Model. *Int. J. Fatigue*, **2010**, *32* (7), 1146–1158. https://doi.org/10.1016/j.ijfatigue.2009.12.013.

[15] Watson, B.; Nandwani, Y.; Worswick, M. J.; Cronin, D. S. Metallic Multi-Material Adhesive Joint Testing and Modeling for Vehicle Lightweighting. *Int. J. Adhes. Adhes.*, **2019**, *95* (August), 102421. https://doi.org/10.1016/j.ijadhadh.2019.102421.

[16] Campilho, R. D. S. G.; Banea, M. D.; Neto, J. A. B. P.; Da Silva, L. F. M. Modelling Adhesive Joints with Cohesive Zone Models: Effect of the Cohesive Law Shape of the Adhesive Layer. *Int. J. Adhes. Adhes.*, **2013**, *44*, 48–56. https://doi.org/10.1016/j.ijadhadh.2013.02.006.

[17] Akhavan-Safar, A.; Monteiro, J.; Carbas, R.; Marques, E.; Goyal, R.; da Silva, L. F. M. Tensile Fatigue Life Prediction of Adhesively Bonded Structures Based on CZM Technique and a Modified Degradation Approach. *Proc. Inst. Mech. Eng. Part G J. Aerosp. Eng.*, **2020**, *234* (13), 1988–1999. https://doi.org/10.1177/0954410020951675.

[18] Watson, B.; Worswick, M. J.; Cronin, D. S. A Novel Cohesive Zone Modelling Approach to Represent Mixed Mode Loading and Bond Line Thickness Effects. *J. Adhes.*, **2023**, *99* (16), 2361–2380. https://doi.org/10.1080/00218464.2023.2184688.

[19] Ibrahim, A. H.; Watson, B.; Jahed, H.; Rezaee, S.; Royer, C.; Cronin, D. S. Prediction of Bonded Asymmetric Metallic Cross-Tension and Single Lap Shear Joints Using Finite Element Model with Material-Level Adhesive Properties and Cohesive Zone Method. *Int. J. Adhes. Adhes.*, **2023**, *120*, 103298. https://doi.org/10.1016/j.ijadhadh.2022.103298.

[20] Watson, B.; Liao, C. H.; Worswick, M. J.; Cronin, D. S. Mode I Traction-Separation Measured Using Rigid Double Cantilever Beam Applied to Structural Adhesive. *J. Adhes.*, **2018**, *96* (8), 717–737. https://doi.org/10.1080/00218464.2018.1502666.

[21] Watson, B.; Worswick, M. J.; Cronin, D. S. Quantification of Mixed Mode Loading and Bond Line Thickness on Adhesive Joint Strength Using Novel Test Specimen Geometry. *Int. J. Adhes. Adhes.*, **2020**, *102* (April), 102682. https://doi.org/10.1016/j.ijadhadh.2020.102682.

[22] Huang, C.; Li, L.; Pichler, N.; Ghafoori, E.; Susmel, L.; Gardner, L. Fatigue Testing and Analysis of Steel Plates Manufactured by Wire-Arc Directed Energy Deposition. *Addit. Manuf.*, **2023**, *73*, 103696. https://doi.org/10.1016/j.addma.2023.103696.

[23] Harris, C. R.; Millman, K. J.; van der Walt, S. J.; Gommers, R.; Virtanen, P.; Cournapeau, D.; Wieser, E.; Taylor, J.; Berg, S.; Smith, N. J.; et al. Array Programming with NumPy. *Nature*, **2020**, *585* (7825), 357–362. https://doi.org/10.1038/s41586-020-2649-2.

[24] Pirondi, A.; Moroni, F. An Investigation of Fatigue Failure Prediction of Adhesively Bonded Metal/Metal Joints. *Int. J. Adhes. Adhes.*, **2009**, *29* (8), 796–805. https://doi.org/10.1016/j.ijadhadh.2009.06.003.

[25] Cui, J.; Wang, S.; Wang, S.; Chen, S.; Li, G. Strength and Failure Analysis of Adhesive Single-Lap Joints under Shear Loading: Effects of Surface Morphologies and Overlap Zone Parameters. *J. Manuf. Process.*, **2020**, *56* (August), 238–247. https://doi.org/10.1016/j.jmapro.2020.04.042.

[26] Asp, L. E.; Sjögren, A.; Greenhalgh, E. S. Delamination Growth and Thresholds in a Carbon/Epoxy Composite under Fatigue Loading. *J. Compos. Technol. Res.*, **2001**, *23* (2), 55–68. https://doi.org/10.1520/ctr10914j.

[27] Kinloch, A. J.; Little, M. S. G.; Watts, J. F. Role of the Interphase in the Environmental Failure of Adhesive Joints. *Acta Mater.*, **2000**, *48* (18–19), 4543–4553. https://doi.org/10.1016/S1359-6454(00)00240-8.

[28] Van Paepegem, W.; Degrieck, J. Fatigue Degradation Modelling of Plain Woven Glass/Epoxy Composites. *Compos. - Part A Appl. Sci. Manuf.*, **2001**, *32* (10), 1433–1441. https://doi.org/10.1016/S1359-835X(01)00042-2.

[29] Alfano, G.; Crisfield, M. A. Finite Element Interface Models for the Delamination Analysis of Laminated Composites: Mechanical and Computational Issues. *Int. J. Numer. Methods Eng.*, **2001**, *50* (7), 1701–1736. https://doi.org/10.1002/nme.93.

[30] Turon, A.; Dávila, C. G.; Camanho, P. P.; Costa, J. An Engineering Solution for Mesh Size Effects in the Simulation of Delamination Using Cohesive Zone Models. *Eng. Fract. Mech.*, **2007**, *74* (10), 1665–1682. https://doi.org/10.1016/j.engfracmech.2006.08.025.